Montagna Symposium on the Biology of Skin

The Skin Immune Atlas: Three-Dimensional Analysis of Cutaneous Leukocyte Subsets by Multiphoton Microscopy

Philip L. Tong[1,2,3], Ben Roediger[1,4], Natasha Kolesnikoff[5], Maté Biro[1,4], Szun S. Tay[1], Rohit Jain[1,4], Lisa E. Shaw[1], Michele A. Grimbaldeston[4] and Wolfgang Weninger[1,2,3]

Site-specific differences in skin response to pathogens and in the course of cutaneous inflammatory diseases are well appreciated. The composition and localization of cutaneous leukocytes has been studied extensively using histology and flow cytometry. However, the precise three-dimensional (3D) distribution of distinct immune cell subsets within skin at different body sites requires visualization of intact living skin. We used intravital multiphoton microscopy in transgenic reporter mice in combination with quantitative flow cytometry to generate a 3D immune cell atlas of mouse skin. The 3D location of innate and adaptive immune cells and site-specific differences in the densities of macrophages, T cells, and mast cells at four defined sites (ear, back, footpad, and tail) is presented. The combinatorial approach further demonstrates an as yet unreported age-dependent expansion of dermal gamma-delta T cells. Localization of dermal immune cells relative to anatomical structures was also determined. Although dendritic cells were dispersed homogeneously within the dermis, mast cells preferentially localized to the perivascular space. Finally, we show the functional relevance of site-specific mast cell disparities using the passive cutaneous anaphylaxis model. These approaches are applicable to assessing immune cell variations and potential functional consequences in the setting of infection, as well as the pathogenesis of inflammatory skin conditions.

Journal of Investigative Dermatology (2015) **135,** 84–93; doi:10.1038/jid.2014.289; published online 14 August 2014

INTRODUCTION

Along with sensory, thermoregulatory, and barrier functions, the skin contains a large repertoire of innate and adaptive immune cells that are responsible for the defense against environmental and microbial insults. The epidermis harbors Langerhans cells (LCs) and, in the mouse, dendritic epidermal T cells (DETCs). In the dermis, macrophages, dermal dendritic cells (DDCs), mast cells, T cells, and other immune cell populations reside in a fibroblast-rich network of collagen and elastin.

Given that the dermis is a structurally nonhomogeneous tissue that contains a large variety of immune cells, it is likely that certain functional leukocyte subsets localize to specific anatomical niches. Support of such cellular and anatomical niches was recently reported, where two distinct fibroblast lineages were found to give rise to the upper dermis, responsible for the dermal papilla and hair follicle formation, and to the lower dermis in murine skin (Driskell *et al.*, 2013). As yet, immune cell composition changes with depth, from the dermal-epidermal junction (DEJ) through to the subcutaneous fat, and its relationship with other anatomical structures, such as the vasculature, has received little attention. Moreover, several novel dermal immune cell subsets (reviewed in Tay *et al.* (2013)) such as DDCs (reviewed in Kaplan (2010)), dermal type 2 innate lymphoid cells (dILC2) (Roediger *et al.*, 2013), and dermal γδ T cells (Sumaria *et al.*, 2011) have only been described very recently, and their precise localization is not entirely clear.

Although the underlying pathomechanisms for the propensity for inflammatory skin diseases to occur at specific predilection sites remain unknown, infection studies suggest intrinsic differences in the skin immune system between different sites. Murine skin infections with *Leishmania major*, for example, lead to functionally divergent outcomes depending upon the site of challenge (Nabors and Farrell, 1994; Nabors *et al.*, 1995; Baldwin *et al.*, 2003; Tabbara *et al.*, 2005). Although not studied systematically, anecdotal evidence suggests that topographical variations in immune cell densities exist for different body sites (Bos, 2004). Mapping cutaneous immune cell compositions topographically therefore has implications for interpreting the context of immune responses during infections and autoimmune diseases.

[1]*Centenary Institute, Newtown, New South Wales, Australia;* [2]*Discipline of Dermatology, The University of Sydney, Camperdown, New South Wales, Australia;* [3]*Department of Dermatology, Royal Prince Alfred Hospital, Camperdown, New South Wales, Australia;* [4]*Sydney Medical School, The University of Sydney, Camperdown, New South Wales, Australia and* [5]*Centre for Cancer Biology, University of South Australia and SA Pathology, Adelaide, South Australia, Australia*

Correspondence: Philip L. Tong or Wolfgang Weninger, Centenary Institute, Locked Bag 6, Newtown, New South Wales 2042, Australia.
E-mail: p.tong@centenary.org.au or w.weninger@centenary.org.au

Abbreviations: 3D, three dimensional; DCC, dermal dendritic cell; DETC, dendritic epidermal T cell; MPM, multiphoton microscopy; SHG, second harmonic generation; YFP, yellow fluorescent protein

Received 16 January 2014; revised 10 April 2014; accepted 29 April 2014; accepted article preview online 9 July 2014; published online 14 August 2014

Central to such investigations is the ability to accurately quantify the numbers and positioning of the relevant immune subpopulations. Although traditional histology and flow cytometric approaches have provided fundamental understanding of the skin immune system, each has certain drawbacks (Emilson and Scheynius, 1995). Tissue processing poses risks of introducing artifacts, for example shrinkage, thereby confounding analysis of anatomical relationships, and also potentially masking epitopes necessary for the proper identification of immune subpopulations by antibodies. Multiparametric flow cytometry allows for the accurate identification and enumeration of even scarce immune cell subsets, however, provides no spatial information while three-dimensional (3D) tissue reconstruction based on serial sections can be limited in scope.

In more recent years, the use of multiphoton microscopy (MPM), in conjunction with fluorescent reporter mice, has enabled the direct and 3D visualization of tagged leukocyte subpopulations within intact skin (Li *et al.*, 2012; Jain and Weninger, 2013). The use of (near)-infrared laser light in MPM allows for deep-tissue imaging with minimal photobleaching and phototoxicity. In addition, the extracellular matrix can be visualized based on second harmonic generation (SHG) signals, thereby providing structural information. Nevertheless, as for other microscopy approaches, MPM relies on cell-specific fluorescent tags within transgenic reporter mice. As transgene expression is seldom restricted to a single immune subpopulation, the accurate enumeration of fluorescent cells requires the combination of MPM with flow cytometry.

Here, we describe the combinatorial approach of incorporating both MPM and flow cytometry to quantify the major leukocyte populations within the epidermis and dermis. We further demonstrate the utility of this method by comparing immune composition between different sites and animal age. This ''Immune Atlas'' provides a platform for the interpretation of site-specific immunity with implications for the understanding of skin physiology, immunopathology, and the actions of therapeutics.

RESULTS

MPM enables the faithful reconstruction of structurally heterogeneous skin sites *in situ*

Structural differences in human skin from different sites have been described at the microscopic and ultrastructural level (Montagna and Parakkal, 1974). Topographical variation in murine skin is less well documented. We focused our study on the mouse ear pinnae, dorsal back, footpad, and tail skin as representative sites of experimental immunological investigations. Structural differences observed in histological sections from hematoxylin and eosin (Supplementary Figure S1a–d online, left column) and Milligan's trichrome stain (Supplementary Figure S1a–d online, middle column) from these sites were detectable with MPM, including the thin epidermis and dermis of ear skin (Supplementary Figure S1a online); the thicker epidermis, dermis, and subcutis of back skin (Supplementary Figure S1b online); the lack of hair follicles in footpads, akin to glabrous skin in humans (Supplementary Figure S1c online); and the thick stratum corneum of footpad and tail skin (Supplementary Figure S1c–d). Confirmation of these structural features with MPM was possible through the imaging of intact skin from transgenic mT/mG mice (Muzumdar *et al.*, 2007), in which all cells express cell membrane–localized red fluorescence (Supplementary Figure S1a–d online, right column). We further visualized extracellular matrix fibers through SHG signals, thereby delineating dermal tissue (Supplementary Figure S1a–d online, right column). Thus, with MPM, we can detect structural features such as epidermal thickness and topography of the DEJ *in situ* without tissue processing or counterstaining to generate 3D tissue stacks of intact murine skin.

Microanatomical specialization of dermal leukocytes at depth and between sites

The spatial distribution of dermal macrophages (Weber-Matthiesen and Sterry, 1990), mast cells (Grimbaldeston *et al.*, 2003; Weber *et al.*, 2003), and T cells (Bos *et al.*, 1987) has been extensively studied in human skin. Whether similar densities and distributions of leukocytes are also found in mouse skin is not known, and this is potentially important given the extensive use of mouse models to study skin diseases. A prerequisite for accurately assessing and quantifying defined, fluorescently-tagged target cell populations in the epidermis and dermis is that fluorescence expression is sufficiently bright to be visualized when analyzing the full thickness of skin by MPM, and that the epidermis and dermis are distinguishable from each other. This led us to select *Cxcr6*$^{+/gfp}$ mice, in which T-cell subsets and dILC2 cells express green fluorescent protein (GFP) (Sumaria *et al.*, 2011; Roediger *et al.*, 2013), and *Csf1r*-enhanced green fluorescent protein (EGFP) (designated hereafter as MacGreen) mice, in which all myeloid cells express GFP (Sasmono *et al.*, 2003). In *Cxcr6*$^{+/gfp}$ mice, CD3^{-}CD2^{+} NK cells also express GFP; however, they are rarely found in the skin under homeostatic conditions (Roediger *et al.*, 2013). No other ILC subsets were observed in the skin during steady state, as confirmed by others (Spencer *et al.*, 2014).

Both LCs and DETCs could be visualized in the epidermis (as defined by the absence of SHG signals (Ng *et al.*, 2008)) of MacGreen and *Cxcr6*$^{+/gfp}$ mice, respectively (Figure 1a, Epidermis). Further, GFP^{+} cells in both MacGreen and *Cxcr6*$^{+/gfp}$ mice could be readily visualized in the dermis (Figure 1a). Although GFP^{+} lymphocytes in *Cxcr6*$^{+/gfp}$ mice were not found at depths greater than 100 μm from the DEJ, myeloid cells including macrophages in MacGreen mice were visible much deeper (up to the cartilage in the ear, Figure 1a, arrowheads, and up to 240 μm at other sites; data not shown). As the GFP fluorescence expression of cells in *Cxcr6*$^{+/gfp}$ mice was comparatively higher than in MacGreen mice, as shown by flow cytometry (1.4–2.9-fold, Supplementary Figure S2a online), we concluded that MPM was sufficient for the detection of deep dermal immune cells.

For accurate enumeration of immune cells by flow cytometry, enzymatic separation of the epidermis and dermis was required (Tschachler *et al.*, 2004). One potential confounding

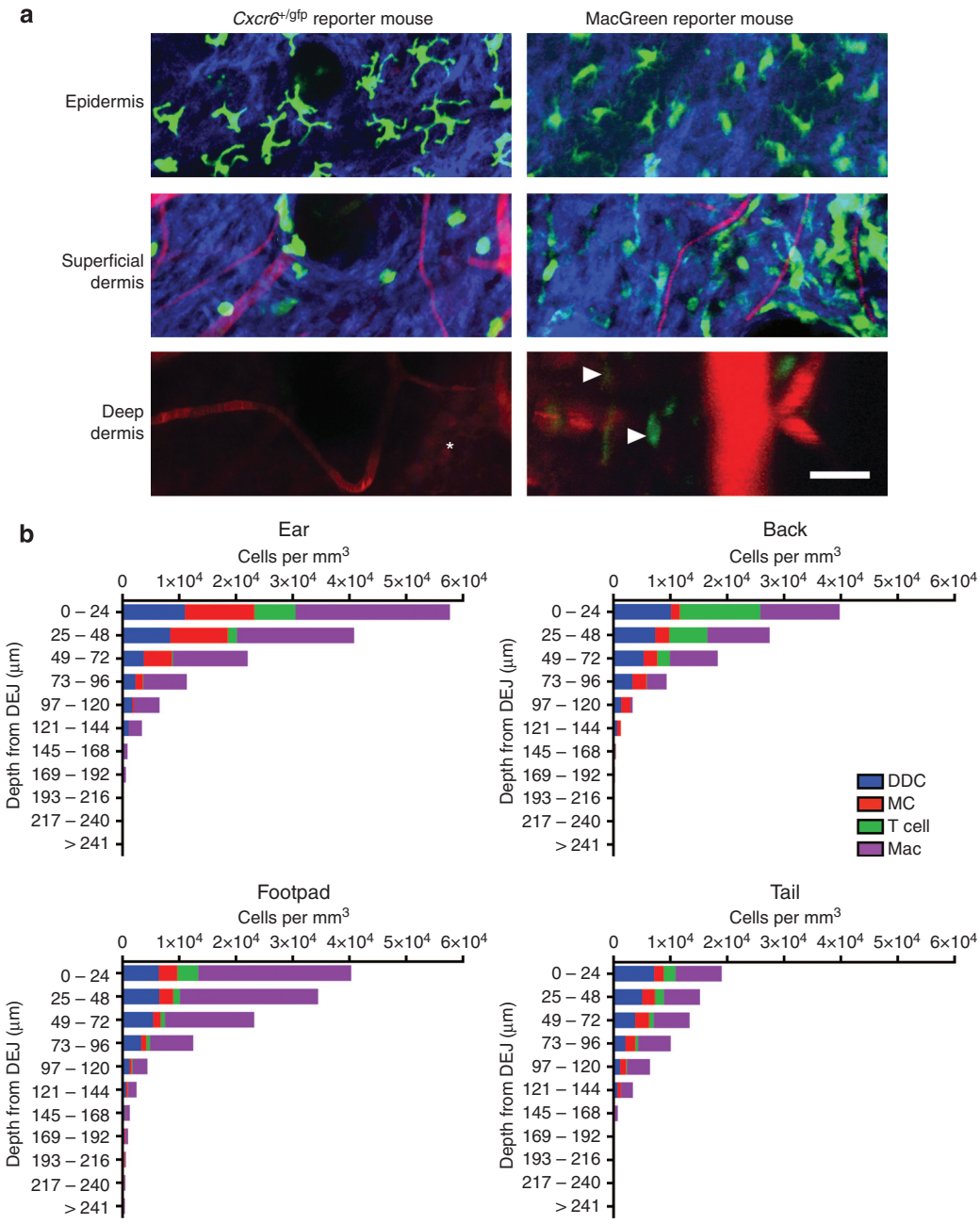

Figure 1. Deep-tissue imaging by multiphoton microscopy demonstrates that spatial distribution of dermal leukocytes differ not only in depth but also between sites. (**a**) Intravital imaging of ear skin of *Cxcr6*$^{+/gfp}$ and *Csf1r*-EGFP (MacGreen) mice at various depths showing green fluorescent protein (GFP)$^{+}$ cells (green) in the deep dermis (arrowheads), extracellular matrix in the dermis (second harmonic generation (SHG) signals, blue), and blood vessels (Evans blue, red). Cartilage is visualized through autofluorescence (asterisk) (representative images from $n=2$ mice per strain). Bar = 50 µm. (**b**) Calculated densities of dermal dendritic cells (DDCs), mast cells (MCs), T cells, and macrophages (Mac) at different sites, stratified by distance from the dermal-epidermal junction (DEJ). $n=3$ for all strains; 6–12 fields of view per site, with flow cytometric adjustment for fluorescence expression with at least 12 mice per strain.

factor with this approach may be their incomplete separation resulting in contamination of either compartment. We first tested efficient separation of the epidermis and dermis by dispase treatment with confocal microscopy (Supplementary Figure S2b online), and found that although the epidermal sheet was effectively removed, pockets of epidermal cells from the hair follicles remained within the dermis. To assess the potential impact of this epidermal component on leukocyte quantification, we enumerated GFP^{+} DETCs and LCs present within hair follicles in *Cxcr6*$^{+/gfp}$ (Sumaria *et al.*, 2011) and MacGreen (Puttur *et al.*, 2010) mice by MPM, respectively. We observed that 1–2% of DETCs and 1–3% of LCs reside within hair follicles when compared with those resident in the interfollicular epidermis (Supplementary Figure S2c–d online). Flow cytometric identification of CD326^{hi} LCs and CD3^{hi} DETCs in both the epidermal and dermal leukocyte

preparations following dispase treatment (Supplementary Figure S2e online) confirmed minimal contamination of the dermal leukocyte preparation with epidermal-derived DETCs and LCs (less than 1% of total $CD45^+$ cells), consistent with the MPM data.

Our combinatorial approach of MPM imaging and flow cytometry was used to enumerate immune cell subsets in the skin. To this end, 3D tissue stacks were obtained by MPM from intact ear, back, footpad, and tail skin in a variety of transgenic reporter mice, and fluorescent cells enumerated post acquisition using image analysis software. We used CD11c-yellow fluorescent protein (YFP), c-Kit-eGFP, *Cxcr6*$^{+/gfp}$, and DPE-GFP mice to determine the spatial distribution of DDCs, mast cells, dermal T cells, and macrophages, respectively (Figure 1b). These mouse strains had been used previously to determine the phenotype, relative proportions, and localization of the respective leukocyte subsets (Ng *et al.*, 2008; Puttur *et al.*, 2010; Sumaria *et al.*, 2011; Roediger *et al.*, 2013; Abtin *et al.*, 2014). The DPE-GFP mouse, driven by the *Cd4* enhancers and promoter (Mempel *et al.*, 2006), also demonstrate GFP expression in αβ T cells and plasmacytoid dendritic cells (Iparraguirre *et al.*, 2008); however, the former can be easily distinguished from the dendritic-like morphology of macrophages as opposed to the rarer ameboid T cells (see Figure 1a, superficial dermis), whereas the latter are not found in the skin under homeostatic conditions (Supplementary Figure S3a online). Furthermore, GFP^+ macrophages in the skin of DPE-GFP mice (Abtin *et al.*, 2014) express GFP at a markedly higher level than skin-resident αβ T cells (Supplementary Figure S3b online). Therefore, only dendritic-like GFP^{hi} cells were enumerated in these mice to quantify macrophages. For the visualization of mast cells, the c-Kit-eGFP mice were specifically used because the GFP expression reported mast cell *Kit* expression (Supplementary Figure S3c online), and not other Kit-expressing cells. Thus, hematopoietic stem cells do not express GFP in these mice, and melanocytes express GFP at two orders of magnitude less than mast cells (Berrozpe *et al.*, 2006). Quantification of the relative percentages of immune cell subsets as determined by flow cytometry was used to adjust numbers obtained by MPM (see Materials and Methods and Supplementary Table S1 online). This combinatorial approach allowed us to calculate the actual density of specific cell subsets per tissue unit (mm^3) stratified at depth.

Our image analyses revealed nonuniform distributions of leukocyte subsets in the vertical direction (Figure 1b). DDCs and dermal T cells resided preferentially within the superficial dermis, whereas macrophages were also found in the deeper regions of the dermis. Mast cells in the ear localized mainly to the superficial dermis, whereas at other sites they were found at similar densities throughout the dermis. Relative proportions of individual leukocyte subsets varied with depth, and these variations differed between sites.

We then compared the densities of LCs (MacGreen mice; Figure 2a), $CD64^-MHC\text{-}II^{hi}$ DDCs (CD11c-YFP mice; Figure 2b), mast cells (c-Kit-eGFP mice; Figure 2c), DETCs (*Cxcr6*$^{+/gfp}$ mice; Figure 2d), $CD3^{int}$ T cells (*Cxcr6*$^{+/gfp}$ mice; Figure 2e), and $CD64^+$ macrophages (DPE-GFP mice; Figure 2f) using the combinatorial approach. To avoid confounding effects of varying epidermal thickness between sites (Supplementary Figure S1 online), LC and DETC density was reported per mm^2 (leukocyte number underlying a mm^2 of skin surface boundary at any depth). Dermal leukocyte density is shown per mm^3 (and per mm^2 in Supplementary Table S2 online, which were comparable with volumetric measurements). We found that mast cells were most prevalent in ear skin, whereas DETCs and dermal T cells were most prevalent in back skin compared with other sites. Higher densities of dermal macrophages were found in ear skin and footpads compared with back skin, whereas DDCs were homogeneous in their distribution, with no site-specific differences observed. LCs were similarly homogeneous in their distribution except for the tail skin, where densities were less than half compared with other sites. Total leukocyte numbers in the epidermis (LCs and DETCs) and dermis (DDCs, mast cells, T cells, and macrophages) were calculated (Figure 2g). The relative site-specific contributions of dermal leukocyte subsets were highly variable, although DDCs and macrophages consistently comprise the majority of dermal leukocytes (Figure 2h).

Quantitative differences in T-cell subsets in ear skin of young and older mice

Given the precision of this approach in quantifying immune cells within the skin, particularly the dermis, we next examined the T-cell composition within the ear in young and old mice. Aging reportedly affects the composition of immune cells, particularly in the adaptive arm, in a variety of organs including skin (reviewed in Sunderkötter, Kalden, and Luger, 1997; Vukmanovic-Stejic *et al.*, 2011). We made use of *Cxcr6*$^{+/gfp}$ mice, and extended our analysis to GFP^+ dermal αβ T cells, γδ T cells, and dILC2 cells (Sumaria *et al.*, 2011; Roediger *et al.*, 2013). MPM was performed *in situ* in 8- to 12-week-old and >12-month-old mice, as shown in Figure 3a. We observed an increased number of GFP^+ cells in the dermis of mice >12 months old and used flow cytometric analysis to determine the composition of dermal lymphocytes by delineating $CD90^{hi}$ leukocytes into dermal αβ T cells, γδ T cells, and dILC2 cell subsets (Supplementary Figure S3d online). Combinatorial MPM and flow cytometry analyses revealed that dermal αβ T cells were significantly increased, whereas dILC2 cells remained largely unaffected by age. Interestingly, and unexpectedly, γδ T cells were also increased in older mice (Figure 3b). The change in αβ T cells may be explained by the fact that T cells in aged mice, similar to humans, display a shift from naïve to memory phenotype during aging (reviewed in Farber *et al.*, 2014).

Quantitative analysis of cell distances to blood vessels demonstrate differences between dermal populations in murine ears *in vivo*

The localization of some immune cell subsets in close proximity to blood vessels has been described on tissue sections (Eady *et al.*, 1979). To quantify the 3D relationship between leukocytes and the vasculature *in vivo*, we developed an image analysis algorithm to automate the measurement of distances of leukocytes to blood vessels in the ear of mice

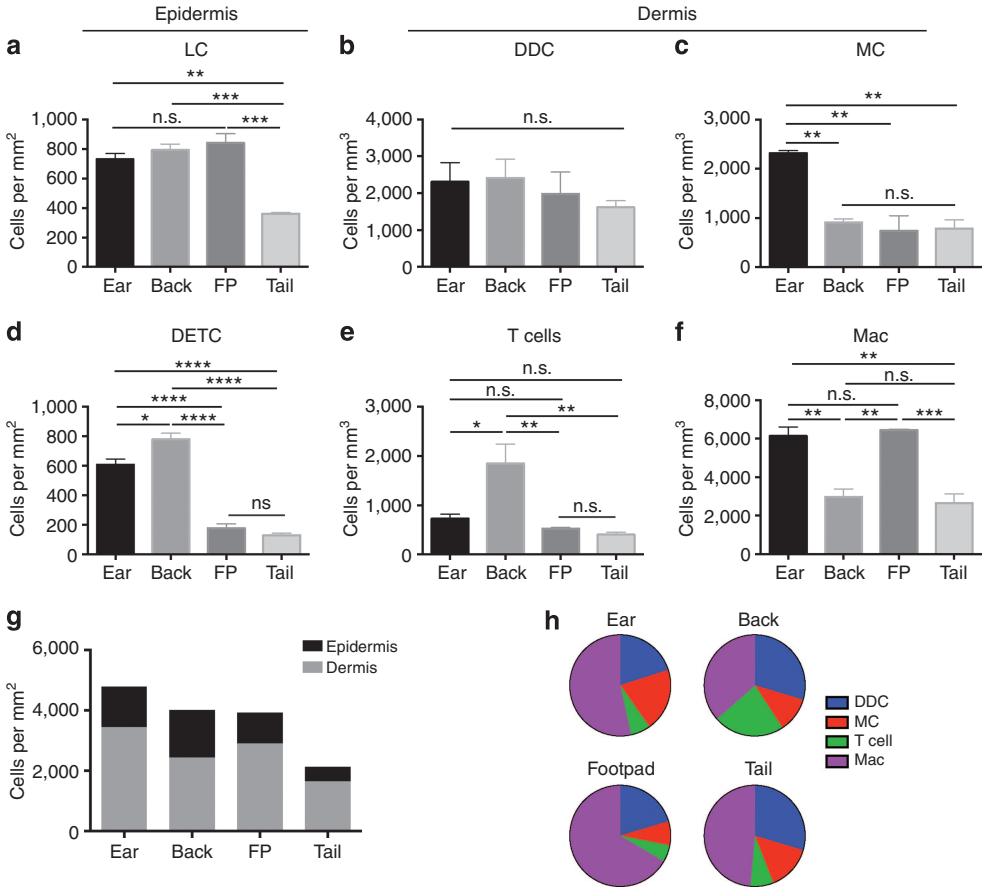

Figure 2. Topographical variation in leukocyte density in the epidermis and dermis. Comparison of leukocyte densities at various cutaneous sites, calculated using the combinatorial approach of multiphoton microscopy (MPM) and flow cytometry. (**a**) Langerhans cells (LCs), (**b**) dermal dendritic cells (DDCs), (**c**) mast cells (MCs), (**d**) dendritic epidermal T cells (DETCs), (**e**) dermal T cells, and (**f**) macrophages (Mac). (**g**) Density of epidermal and dermal leukocytes at various cutaneous sites and (**h**) proportion of indicated dermal leukocytes according to site. Data are mean ± SEM ($n = 3$ for all strains, 6–12 fields of view per site, with flow cytometric adjustment for fluorescence expression with at least 12 mice per strain; one-way analysis of variance (ANOVA) with Tukey's *post hoc* test). *$P<0.05$, **$P<0.01$, ***$P<0.001$, ****$P<0.0001$; n.s., not significant.

under live imaging conditions (see Supplementary Materials and Methods; freely available at http://www.matebiro.com/software/immuneatlas). We included mast cells, which are largely nonmigratory (Figure 4a, top row), and DDCs, which show constitutive migration within noninflamed dermis (Ng *et al.*, 2008) (Figure 4a, bottom row). We found that 54.2% and 36.4% of mast cells and DDCs, respectively, resided within 10 μm of the nearest blood vessel (Figure 4b). Overall, differences in cell-to-blood vessel distances for mast cells and DDCs were highly significant (Figure 4c), confirming the nonhomogeneous distribution of individual leukocyte subsets in the dermis by live imaging.

Site-specific differences in mast cell numbers associate with functionally distinct immune responses

Finally, we set out to determine whether variations in densities of leukocyte subsets paralleled differences in immune reactions between these sites. We focused on mast cells, based upon clear disparity in densities between ear and back skin by MPM (Figure 2c and 5a), and confirmed by toluidine blue staining on histological sections (Figure 5a) (Grimbaldeston *et al.*, 2005). Mast cells contribute to allergic responses through IgE-mediated release of preformed mediators such as histamine—a potent mediator of vascular permeability (reviewed in Galli and Tsai, 2012). Therefore, we used the passive cutaneous anaphylaxis model (Wershil *et al.*, 1991), a test for mast cell function *in vivo*. Antigen-specific IgE was injected intradermally in the ear and dorsal back in albino C57BL/6-*Tyr*$^{c\text{-}2J}$/J mice. The antigen and Evans blue dye was injected intravenous 16 hours later, resulting in histamine release, vascular leakage, and dye extravasation (Figure 5b). Mast cell–deficient C57BL/6J-*Kit*$^{W\text{-}sh/W\text{-}sh}$ mice were used as a negative control (Figure 5b). We observed increased dye extravasation in the ear compared with the back (Figure 5c), consistent with the higher numbers of mast cells in ear skin. This difference was not seen in vehicle controls or in C57BL/6J-*Kit*$^{W\text{-}sh/W\text{-}sh}$ mice (Figure 5b), confirming that Evans blue leakage was mast cell dependent. Thus, there is a functional correlation between the density of mast cells and dye leakage after experimental passive cutaneous anaphylaxis.

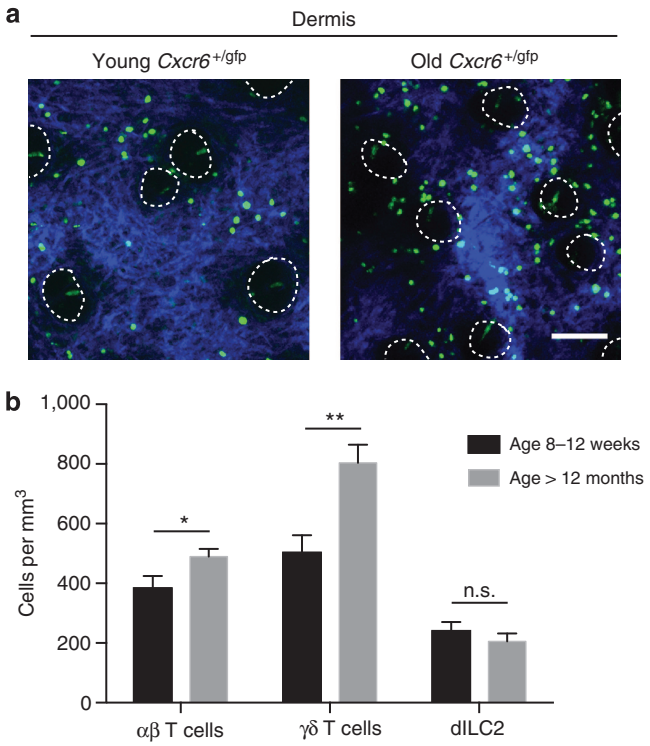

Figure 3. Quantification of group 2 innate lymphoid cells and αβ and γδ T cells in ear skin of young and aged mice. (**a**) Representative ($n > 8$ per age group) images of green fluorescent protein (GFP)$^+$ cells (green) in young (8–12 weeks) and older ear dermis (>12 months) of *Cxcr6*$^{+/gfp}$ mice with extracellular matrix (ECM) in the dermis (second harmonic generation (SHG) signals, blue) and dotted lines to indicate hair follicles. (**b**) Density of indicated populations in *Cxcr6*$^{+/gfp}$ mouse ear skin in mice aged 8–12 weeks and greater than 12 months. Results are pooled from three independent experiments (>8 mice per age group). Data are mean ± SEM and represent averaged flow-adjusted densities from both ears of each mouse. $^{**}P < 0.01$; n.s., not significant (unpaired *t*-test). Bar = 100 μm.

DISCUSSION

The mechanisms underlying regional immunity, that is, differences in the quality of immune responses between different organs such as the gut and the skin, are increasingly recognized (Sathaliyawala *et al.*, 2013). We now further appreciate that, within a given organ, immune cell populations can be heterogeneous in composition. The skin is a good example in this context, and has served as a widely used paradigm to study regional immunity and the specialized functions of leukocyte subsets. Our results suggest layers of complexity to the immune microcosm in the skin, namely site-specific differences in immune cell density. Furthermore, the differences seen in mast cell density suggest that cutaneous immune responses indeed may display site-specific functional reactivity. This complexity also extends to the nonhomogeneous arrangement and relative proportions of distinct populations of immune cells based on tissue depth, which may have implications for the ensuing immune response upon pathogen entry into the skin.

Our intravital imaging approach represents a methodological advance, as it circumvents technical challenges of conventional histologic approaches, such as sample shrinkage and tissue processing artifacts. In combination with multiparameter flow cytometry, MPM enabled quantification of densities of several leukocyte subsets in the skin at different depths (up to 240 μm from the DEJ) including the epidermis. We found that the spatial distribution of dermal leukocytes was significantly region-specific. However, similarities between sites included DDCs and T cells residing in the superficial dermis, whereas macrophages and mast cells were generally distributed throughout the entire dermis. Our data confirm the spatial distribution of human dermal macrophages (Weber-Matthiesen and Sterry, 1990) and mast cells (Grimbaldeston *et al.*, 2003; Weber *et al.*, 2003). We consistently found accumulation of T cells directly underneath the murine epidermis, which, in contrast to human studies, are reported to distribute throughout the dermis (Bos *et al.*, 1987). We further corroborate the close association of mast cells, in contrast to DDCs, with blood vessels. Finally, the combinatorial approach used in this study quantified individual T-cell subsets and revealed that γδ T cells are numerically increased in the skin of aged mice. Until recently, γδ T cells were thought to be a purely innate immune population. However, recent studies indicate they are capable of exhibiting hallmarks of memory, as demonstrated in the intestine after *Listeria monocytogenes* infection (Sheridan *et al.*, 2013) and in the peritoneal cavity after *Staphylococcus aureus* infection (Murphy *et al.*, 2014). Our results raise the intriguing possibility that dermal γδ T cells, which represent a distinct but nevertheless polyclonal γδ T-cell population (Sumaria *et al.*, 2011), may also be capable of exhibiting memory. Collectively, our results demonstrate the suitability of our combinatorial approach to the quantification of numerous immune cell subpopulations within the skin across a range of sites and experimental conditions.

Recently, Wang *et al.* (2014) used 3D microscopy in human skin using whole-mount immunofluorescence staining of dendritic cells, macrophages, and T cells. They demonstrated distinct microanatomical localization of these cells depending on tissue depth. Although their study used skin harvested from breast reduction surgery and quantified up to a depth of 60 μm, as well as greater than 150 μm from the DEJ, their data were consistent with our results in murine skin. Nevertheless, they describe cord-like perivascular distribution of dermal leukocytes past a depth of 150 μm from the DEJ. Although we occasionally see T cells and mast cells in footpad skin *in situ* arranged in a perivascular manner in the deep dermis, this is rather an exception. It remains to be confirmed whether these observed differences relate to different techniques used to highlight leukocytes, sample processing of human tissue, or true species differences. In the future, our customized image analysis package can be applied to whole human skin that is similarly stained, but 'optically cleared' (reviewed in Zhu *et al.*, 2013), to ensure that no cell escapes detection.

Despite the strengths of the described combinatorial approach, criteria must be met in order for it to be used effectively. The depth of microscopic examination and therefore tissue thickness affects the ability for fluorescence to be

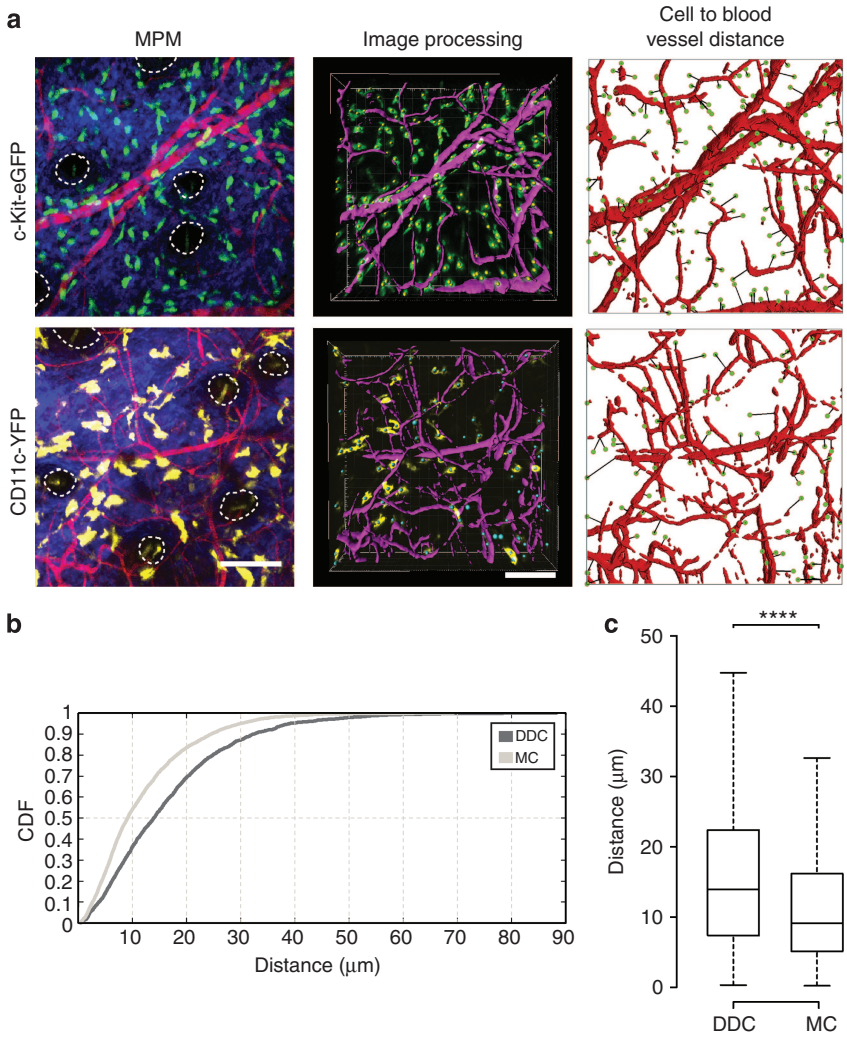

Figure 4. Customized automated cell-to-blood vessel distance analysis of a migratory and nonmigratory dermal population. (**a**) Left: representative intravital multiphoton microscopy (MPM) images of c-Kit-eGFP and CD11c-YFP ear skin showing green fluorescent protein (GFP)$^+$ mast cells (MCs; top, green), YFP$^+$ dermal dendritic cells (DDCs; bottom, yellow), extracellular matrix (second harmonic generation (SHG) signals, blue), and vasculature (Evans blue, red). Middle: computer-assisted recognition of cells (spots, yellow, or green) and vasculature (purple). Right: calculations of distances from every cell to the nearest blood vessels (path in black). (**b**) Cumulative distribution function (CDF) of the nearest distances of MCs and DDCs to vasculature in c-Kit-eGFP and CD11c-YFP mice, respectively (in µm). (**c**) Box-whisker plot of cell-to-blood vessel distance in indicated populations (outliers excluded). $n=3$ mice; 27 fields of view per strain; >2,000 cells examined; ****$P<0.0001$ (Mann–Whitney U-test). Bar = 100 µm.

detected. These factors may change in physiological (e.g., different body sites) and pathological states (e.g., inflammation). To be confident of quantification, the entire dermis needs to be visualized and thus it may not be applicable in skin with severe inflammation or excessive epidermal thickening. Despite remaining challenges, our method has potential applications for developmental studies (e.g., using knockout mice) and a range of experimental conditions, where sensitive and accurate immune cell quantification is required.

Further, completing the skin ''Immune Atlas'' will require comprehensive topographical and spatial detailing of lymphatics and nerves (Tschachler *et al.*, 2004) and their association with dermal leukocytes. Potential approaches include labeling of these structures *in vivo* for simultaneous visualization with leukocytes (Kilarski *et al.*, 2013). Although *in vivo* examination of human skin is still in its infancy, exploiting inherent physical properties of tissue through second- and third-harmonic generation signals may allow a human atlas of skin to be developed (Rehberg *et al.*, 2011; Tong *et al.*, 2013). The systematic combinatorial approach that we describe would enable confirmation of earlier studies documenting the effect of UV radiation on regional variation in leukocyte density (Bergstresser *et al.*, 1980). Applications include evaluating the skin microbiome, known to be topographically diverse and to extend below the DEJ (Nakatsuji *et al.*, 2013), and its possible influence on leukocyte diversity in the epidermis and dermis. This may have therapeutic implications when microflora are altered in the setting of certain inflammatory skin disorders (reviewed in Grice and Segre, 2011; Schommer and Gallo, 2013).

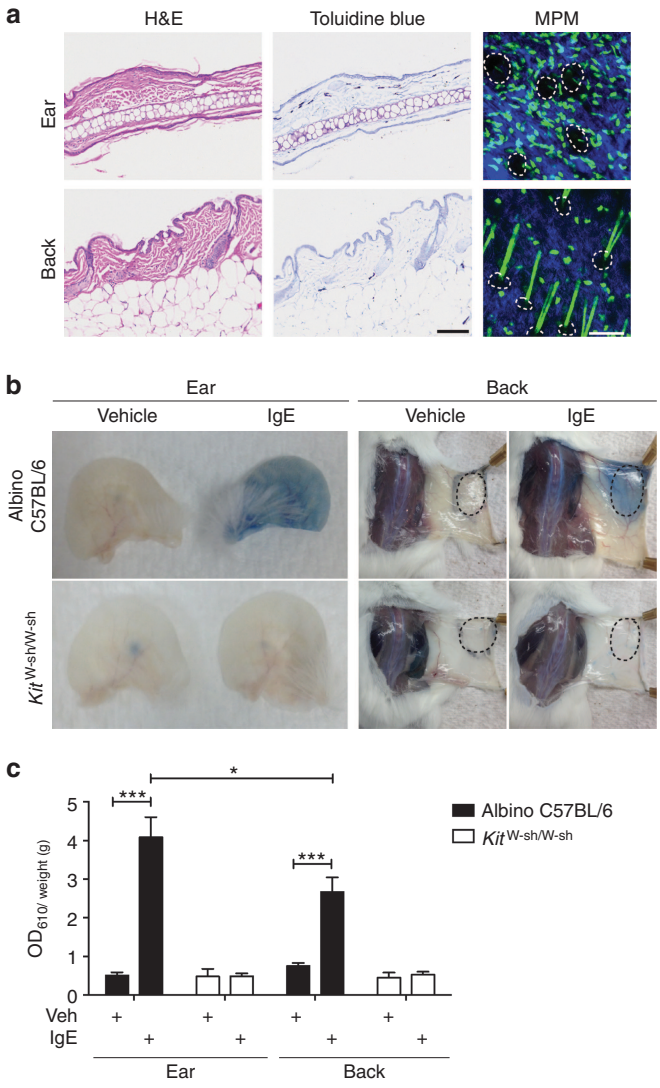

Figure 5. Site-specific differences in mast cell numbers quantified by multiphoton imaging and the passive cutaneous anaphylaxis functional assay. (**a**) Histology from albino C57BL/6-*Tyr*$^{c\text{-}2J}$/J ear or back skin stained with hematoxylin and eosin (H&E) and toluidine blue; multiphoton microscopy (MPM) of c-Kit-eGFP ear or back skin demonstrating green fluorescent protein (GFP)$^{+}$ mast cells (green), extracellular matrix (second harmonic generation (SHG) signals, blue), and hair follicles (dotted lines). (**b**) Ear and back skin of albino C57BL/6-*Tyr*$^{c\text{-}2J}$/J or mast cell–deficient C57BL/6J-*Kit*$^{W\text{-}sh/W\text{-}sh}$ mice treated with vehicle or IgE anti-DNP (intradermal (i.d.) injection site, dotted lines) and challenged 16 hours later with intravenous (i.v.) DNP-HSA containing Evans blue dye. (**c**) Dye extravasation (weight adjusted) for indicated sites and strains quantified by absorption at 610 nm (one-way analysis of variance (ANOVA) with Dunnett's *post hoc* test). Data are mean ± SD; $*P<0.05$; $***P<0.001$. Bar = 100 μm. Data representative of (**a**) three mice per strain, (**b**, **c**) >3 mice per strain per site.

In summary, we describe a robust and versatile quantification technique to investigate the immune system of the skin by incorporating multiphoton imaging data and correcting for nonuniform fluorescence expression in transgenic reporter mice with multiparameter flow cytometry. The result is the comprehensive mapping of the skin immune system in 3D, accessible to investigators for dissecting the immune response in skin for a better understanding of physiological and pathological changes during infection and autoimmunity.

MATERIALS AND METHODS

Mice

C57BL/6 mice were obtained from the Animal Research Centre in Perth, Australia. Albino C57BL/6 (B6(Cg)-*Tyr*$^{c\text{-}2J}$/J), *Cxcr6*$^{+/gfp}$, and mT/mG mice (Muzumdar *et al.*, 2007) were purchased from the Jackson Laboratory (Bar Harbor, ME). CD11c-YFP mice (Lindquist *et al.*, 2004) were a gift from M. Nussenzweig. The c-Kit-eGFP mice (Berrozpe *et al.*, 2006) were a gift from P. Besmer. The *Csf1r*-EGFP (MacGreen) mice (Sasmono *et al.*, 2003) were a gift from D. Hume. DPE-GFP mice have been described previously (Mempel *et al.*, 2006). Mice were bred and maintained on the C57BL/6 background in pathogen-free conditions at the Centenary Institute animal facility. *Kit*$^{W\text{-}sh/W\text{-}sh}$ (Grimbaldeston *et al.*, 2005) backcrossed 14 generations to C57BL/6J mice and also albino C57BL/6(Cg)-*Tyr*$^{c\text{-}2J}$/J were bred and maintained at the Institute of Medical and Veterinary Science animal facility, Adelaide, Australia. All experiments performed were approved by the Animal Ethics Committees at the University of Sydney (Sydney, Australia), Royal Prince Alfred Hospital (Sydney, Australia), and the Institute of Medical and Veterinary Science Animal Ethics Committee (Adelaide, Australia).

Multiphoton imaging

A combination of *ex vivo* and *in vivo* imaging of murine skin was performed. For *in vivo* imaging, mice were anesthetized with Ketamine/Xylazine (80/10 mg kg^{-1}, intraperitoneal) with repeated half doses as required. The anesthetized mouse was mounted on a custom-built ear stage with its body temperature controlled as described previously (Ng *et al.*, 2008; Li *et al.*, 2012). MPM was performed on a custom-built TriMScope (LaVision BioTec, Bielefeld, Germany) attached to an Olympus BX-51 fixed-stage microscope equipped with either a ×16 (Nikon LWD, numerical aperture 0.80; Nikon, Tokyo, Japan) or ×20 (Olympus XLUMPlanFl IR coated, numerical aperture 0.95; Olympus, Center Valley, PA) water-immersion objective. For *ex vivo* imaging, mice were euthanized using CO_2 asphyxiation, hair was removed with Nair, and tissues were harvested from the ear, dorsal back, footpad, and tail skin. A wideband mode-locked Ti:sapphire femtosecond laser (Mai Tai HP/Spectra-Physics; Newport, Irvine, CA) was used to excite the skin at a wavelength of 920 nm or 940 nm for imaging of GFP and YFP, respectively. Blood vessels were visualized through intravenous (tail vein) injection of Evans blue (Gurr-Searle Diagnostic) conjugated to BSA (Abtin *et al.*, 2014).

The combinatorial approach using MPM and flow cytometry for enumeration of actual epidermal and dermal leukocyte densities in transgenic fluorescent mice *in situ*

Image stacks were acquired from MacGreen, CD11c-YFP, c-Kit-eGFP, DPE-GFP, and *Cxcr6*$^{+/gfp}$ mice to enumerate LCs, DDCs, mast cells, macrophages, and lymphoid populations (which include DETCs, dermal T cells, and dILC2), respectively. All images obtained were 300 × 300 μm or 400 × 400 μm in the *X*–*Y* direction with a pixel resolution of 500 × 500 pixels. In total, 2- or 4-μm spacing in the *z* axis was used through the entire depth of the tissue (up to 300 μm from the epidermis). Incrementing power when imaging deeper into the skin was facilitated through the ImSpector Software (Göttingen,

Germany). Images were counted manually using the 'multi-point' selection tools (ImageJ, US National Institutes of Health) to determine the density of GFP^+/YFP^+ cells. The expression of fluorescent reporter genes by flow cytometry was obtained from ear skin samples and used to adjust the density of epidermal and dermal leukocytes for all skin sites. All GFP^+ cells in c-Kit-eGFP mice were mast cells (Supplementary Figure S3c online; Berrozpe *et al.*, 2006), and all GFP^+ cells in the epidermis in MacGreen mice were MHC-$II^{hi}CD326^+$ LCs (Puttur *et al.* 2010). The other reporter mice used in this study required adjustment to determine the actual density based on the fact that $64 \pm 4.4\%$ of $CD64^-$MHC-II^{hi} DCs expressed YFP in CD11c-YFP mice, whereas $42 \pm 10.5\%$ of $CD64^+$ macrophages were GFP^+ in DPE-GFP mice. In *Cxcr6*$^{+/gfp}$ mice, GFP expression was observed in all $CD3^{hi}$ DETCs and $72 \pm 5.2\%$ of dermal $CD90^{hi}CD3^{int}$ T cells. Leukocyte density was determined as follows: density of cell A = (density GFP^+ cells) × (percentage of GFP^+ cells of cell type A)÷(percentage of cell type A that are GFP^+) (see also Supplementary Table S1 online). Data were normalized to per mm^2 or per mm^3.

CONFLICT OF INTEREST

The authors state no conflict of interest.

ACKNOWLEDGMENTS

We thank the staff of the Advanced Cytometry Facility and Imaging Core Facilities at Centenary Institute, Y. Wen Loh, and L. Ittner for their technical assistance. MB acknowledges Bitplane for supplying a full developer license for Imaris. PLT was supported by a NHMRC Postgraduate Scholarship. WW and MB are Fellows of the Cancer Institute New South Wales. MB was supported by grant 1070498 from the Cure Cancer Australia Foundation and an ECR grant from Sydney Medical School, University of Sydney. MAG is a NHMRC Career Development Fellow. This work was funded by the NHMRC (1066477, 1047041, 1011203) and the Australian Research Council. Publication costs were funded by the NIH (R13-AR009431-48).

SUPPLEMENTARY MATERIAL

Supplementary material is linked to the online version of the paper at http://www.nature.com/jid

REFERENCES

Abtin A, Jain R, Mitchell AJ *et al.* (2014) Perivascular macrophages mediate neutrophil recruitment during bacterial skin infection. *Nat Immunol* 15:45–53

Baldwin TM, Elso C, Curtis J *et al.* (2003) The site of *Leishmania major* infection determines disease severity and immune responses. *Infect Immun* 71:6830–4

Bergstresser PR, Toews GB, Streilein JW (1980) Natural and perturbed distributions of Langerhans cells: responses to ultraviolet light, heterotopic skin grafting, and dinitrofluorobenzene sensitization. *J Invest Dermatol* 75:73–7

Berrozpe G, Agosti V, Tucker C *et al.* (2006) A distant upstream locus control region is critical for expression of the Kit receptor gene in mast cells. *Mol Cell Biol* 26:5850–60

Bos JD (ed) (2004) *Skin Immune System: Cutaneous Immunology and Clinical Immunodermatology*. 3rd edn. CRC Press, 840

Bos JD, Zonneveld I, Das PK *et al.* (1987) The skin immune system (SIS): distribution and immunophenotype of lymphocyte subpopulations in normal human skin. *J Invest Dermatol* 88:569–73

Driskell RR, Lichtenberger BM, Hoste E *et al.* (2013) Distinct fibroblast lineages determine dermal architecture in skin development and repair. *Nature* 504:277–81

Eady RA, Cowen T, Marshall TF *et al.* (1979) Mast cell population density, blood vessel density and histamine content in normal human skin. *Br J Dermatol* 100:623–33

Emilson A, Scheynius A (1995) Quantitative and three-dimensional analysis of human Langerhans cells in epidermal sheets and vertical skin sections. *J Histochem Cytochem* 43:993–8

Farber DL, Yudanin NA, Restifo NP (2014) Human memory T cells: generation, compartmentalization and homeostasis. *Nat Rev Immunol* 14: 24–35

Galli SJ, Tsai M (2012) IgE and mast cells in allergic disease. *Nat Med* 18: 693–704

Grice EA, Segre JA (2011) The skin microbiome. *Nat Rev Microbiol* 9:244–53

Grimbaldeston MA, Chen CC, Piliponsky AM *et al.* (2005) Mast cell-deficient W-sash c-kit mutant Kit W-sh/W-sh mice as a model for investigating mast cell biology *in vivo*. *Am J Pathol* 167:835–48

Grimbaldeston MA, Simpson A, Finlay-Jones JJ *et al.* (2003) The effect of ultraviolet radiation exposure on the prevalence of mast cells in human skin. *Br J Dermatol* 148:300–6

Iparraguirre A1, Tobias JW, Hensley SE *et al.* (2008) Two distinct activation states of plasmacytoid dendritic cells induced by influenza virus and CpG 1826 oligonucleotide. *J Leukoc Biol* 83:610–20

Jain R, Weninger W (2013) Shedding light on cutaneous innate immune responses: the intravital microscopy approach. *Immunol Cell Biol* 91:263–70

Kaplan DH (2010) *In vivo* function of Langerhans cells and dermal dendritic cells. *Trends Immunol* 31:446–51

Kilarski WW, Güç E, Teo JC *et al.* (2013) Intravital immunofluorescence for visualizing the microcirculatory and immune microenvironments in the mouse ear dermis. *PLoS ONE* 8:e57135

Li JL, Goh CC, Keeble JL *et al.* (2012) Intravital multiphoton imaging of immune responses in the mouse ear skin. *Nat Protoc* 7:221–34

Lindquist RL, Shakhar G, Dudziak D *et al.* (2004) Visualizing dendritic cell networks *in vivo*. *Nat Immunol* 5:1243–50

Mempel TR, Pittet MJ, Khazaie K *et al.* (2006) Regulatory T cells reversibly suppress cytotoxic T cell function independent of effector differentiation. *Immunity* 25:129–41

Montagna W, Parakkal PF (eds) (1974) *The Structure and Function of Skin*. Academic Press: London, 448

Murphy AG, O'Keeffe KM, Lalor SJ *et al.* (2014) *Staphylococcus aureus* infection of mice expands a population of memory γδ T cells that are protective against subsequent infection. *J Immunol* 192:3697–708

Muzumdar MD, Tasic B, Miyamichi K *et al.* (2007) A global double-fluorescent Cre reporter mouse. *Genesis* 45:593–605

Nabors GS, Farrell JP (1994) Site-specific immunity to Leishmania major in SWR mice: the site of infection influences susceptibility and expression of the antileishmanial immune response. *Infect Immun* 62: 3655–62

Nabors GS, Nolan T, Croop W *et al.* (1995) The influence of the site of parasite inoculation on the development of Th1 and Th2 type immune responses in (BALB/c x C57BL/6) F1 mice infected with *Leishmania major*. *Parasite Immunol* 17:569–79

Nakatsuji T, Chiang HI, Jiang SB *et al.* (2013) The microbiome extends to subepidermal compartments of normal skin. *Nat Commun* 4:1431

Ng LG, Hsu A, Mandell MA *et al.* (2008) Migratory dermal dendritic cells act as rapid sensors of protozoan parasites. *PLoS Pathog* 4:e1000222

Puttur FK, Fernandez MA, White R *et al.* (2010) Herpes simplex virus infects skin gamma delta T cells before Langerhans cells and impedes migration of infected Langerhans cells by inducing apoptosis and blocking E-cadherin downregulation. *J Immunol* 185:477–87

Roediger B, Kyle R, Yip KH *et al.* (2013) Cutaneous immunosurveillance and regulation of inflammation by group 2 innate lymphoid cells. *Nat Immunol* 14:564–73

Rehberg M, Krombach F, Pohl U *et al.* (2011) Label-free 3D visualization of cellular and tissue structures in intact muscle with second and third harmonic generation microscopy. *PLoS ONE* 6:e28237

Sasmono RT, Oceandy D, Pollard JW *et al.* (2003) A macrophage colony-stimulating factor receptor-green fluorescent protein transgene is expressed throughout the mononuclear phagocyte system of the mouse. *Blood* 101:1155–63

Sathaliyawala T, Kubota M, Yudanin N *et al.* (2013) Distribution and compartmentalization of human circulating and tissue-resident memory T cell subsets. *Immunity* 38:187–97

Schommer NN, Gallo RL (2013) Structure and function of the human skin microbiome. *Trends Microbiol* 21:660–8

Sheridan BS, Romagnoli PA, Pham QM *et al.* (2013) γδ T cells exhibit multifunctional and protective memory in intestinal tissues. *Immunity* 39:184–95

Spencer SP, Wilhelm C, Yang Q *et al.* (2014) Adaptation of innate lymphoid cells to a micronutrient deficiency promotes type 2 barrier immunity. *Science* 343:432–7

Sumaria N, Roediger B, Ng LG *et al.* (2011) Cutaneous immunosurveillance by self-renewing dermal gammadelta T cells. *J Exp Med* 208: 505–18

Sunderkötter C, Kalden H, Luger TA (1997) Aging and the skin immune system. *Arch Dermatol* 133:1256–62

Tabbara KS, Peters NC, Afrin F *et al.* (2005) Conditions influencing the efficacy of vaccination with live organisms against *Leishmania major* infection. *Infect Immun* 73:4714–22

Tay SS, Roediger B, Tong PL *et al.* (2013) The skin-resident immune network. *Curr Derm Rep* 3:13–22

Tong PL, Qin J, Cooper CL *et al.* (2013) A quantitative approach to histopathological dissection of elastin-related disorders using multiphoton microscopy. *Br J Dermatol* 169:869–79

Tschachler E, Reinisch CM, Mayer C *et al.* (2004) Sheet preparations expose the dermal nerve plexus of human skin and render the dermal nerve end organ accessible to extensive analysis. *J Invest Dermatol* 122:177–82

Vukmanovic-Stejic M, Rustin MH, Nikolich-Zugich J *et al.* (2011) Immune responses in the skin in old age. *Curr Opin Immunol* 23:525–31

Wang XN, McGovern N, Gunawan M *et al.* (2014) A three-dimensional atlas of human dermal leukocytes, lymphatics, and blood vessels. *J Invest Dermatol* 134:965–74

Weber A, Knop J, Maurer M (2003) Pattern analysis of human cutaneous mast cell populations by total body surface mapping. *Br J Dermatol* 148:224–8

Weber-Matthiesen K, Sterry W (1990) Organization of the monocyte/macrophage system of normal human skin. *J Invest Dermatol* 95:83–9

Wershil BK, Wang ZS, Gordon JR *et al.* (1991) Recruitment of neutrophils during IgE-dependent cutaneous late phase reactions in the mouse is mast cell-dependent. Partial inhibition of the reaction with antiserum against tumor necrosis factor-alpha. *J Clin Invest* 87:446–53

Zhu D, Larin KV, Luo Q *et al.* (2013) Recent progress in tissue optical clearing. *Laser Photon Rev* 7:732–57